

## Geomagnetically trapped light isotopes observed with the detector NINA

A. Bakaldin,<sup>1</sup> A. Galper,<sup>1</sup> S. Koldashov,<sup>1</sup> M. Korotkov,<sup>1</sup> A. Leonov,<sup>1</sup> V. Mikhailov,<sup>1</sup> A. Murashov,<sup>1</sup> S. Voronov,<sup>1</sup> V. Bidoli,<sup>2</sup> M. Casolino,<sup>2</sup> M. De Pascale,<sup>2</sup> G. Furano,<sup>2</sup> A. Iannucci,<sup>2</sup> A. Morselli,<sup>2</sup> P. Picozza,<sup>2</sup> R. Sparvoli,<sup>2</sup> M. Boezio,<sup>3</sup> V. Bonvicini,<sup>3</sup> R. Cirami,<sup>3</sup> A. Vacchi,<sup>3</sup> N. Zampa,<sup>3</sup> M. Ambriola,<sup>4</sup> R. Bellotti,<sup>4</sup> F. Cafagna,<sup>4</sup> F. Ciaccio,<sup>4</sup> M. Circella,<sup>4</sup> C. De Marzo,<sup>4</sup> O. Adriani,<sup>5</sup> P. Papini,<sup>5</sup> P. Spillantini,<sup>5</sup> S. Straulino,<sup>5</sup> E. Vannuccini,<sup>5</sup> M. Ricci,<sup>6</sup> and G. Castellini<sup>7</sup>

Received 4 July 2001; revised 26 October 2001; accepted 1 November 2001; published 7 August 2002.

[1] The detector New Instrument for Nuclear Analysis (NINA) aboard the satellite Resurs-01-N4 detected hydrogen and helium isotopes geomagnetically trapped, while crossing the South Atlantic Anomaly. Deuterium and tritium at  $L$  shell  $< 1.2$  were unambiguously recognized. The  ${}^3\text{He}$  and  ${}^4\text{He}$  power law spectra, reconstructed at  $L$  shell = 1.2 and  $B < 0.22$  G, have indices equal to  $2.30 \pm 0.08$  in the energy range 12–50 MeV nucleon<sup>-1</sup> and  $3.4 \pm 0.2$  in 10–30 MeV nucleon<sup>-1</sup>, respectively. The measured  ${}^3\text{He}/{}^4\text{He}$  ratio and the reconstructed deuterium profile as a function of  $L$  shell bring one to the conclusion that the main source of radiation belt light isotopes at Resurs altitudes ( $\sim 800$  km) and for energy greater than 10 MeV nucleon<sup>-1</sup> is the interaction of trapped protons with residual atmospheric helium. *INDEX TERMS:* 2720 Magnetospheric Physics: Energetic particles, trapped; 2730 Magnetospheric Physics: Magnetosphere—inner; 2794 Magnetospheric Physics: Instruments and techniques; *KEYWORDS:* trapped energetic particles, isotopes, silicon detector

### 1. Introduction

[2] The trapped helium component in Earth's radiation belts was discovered at the beginning of the 1960s [*Krimigis and Van Allen*, 1967]. Its isotopic composition was studied many years later with the ONR-604 instrument on board the Combined Release and Radiation Effects Satellite (CRRES), in the energy range 50–100 MeV nucleon<sup>-1</sup> [*Wefel et al.*, 1995] and with the spectrometer Mass Spectrometer Telescope (MAST) on board Solar, Anomalous, Magnetospheric Particle Explorer (SAMPEX) in the interval 5–15 MeV nucleon<sup>-1</sup> [*Selesnick and Mewaldt*, 1996]. It was found that  ${}^3\text{He}$  is more abundant than  ${}^4\text{He}$  in the inner radiation belt, at least for  $L$  shell  $< 1.5$ . The CRRES measured  ${}^3\text{He}/{}^4\text{He}$  averaged ratio in the energy interval 51–86 MeV nucleon<sup>-1</sup> was  $8.7 \pm 3.1$  at  $L$  shell 1.1  $\div$  1.5 and  $2.4 \pm 0.6$  at  $L$  shell 1.5  $\div$  2.3 [*Wefel et al.*, 1995]; this ratio decreases as a function of energy in the first  $L$  shell

range and increases in the second. At  $L$  shell 1.1  $\div$  1.5 the power law fit gives spectral indices equal to  $5.9 \pm 0.4$  for  ${}^3\text{He}$  and  $4.1 \pm 0.3$  for  ${}^4\text{He}$ . The  ${}^3\text{He}/{}^4\text{He}$  ratio obtained on board SAMPEX at  $L$  shell = 1.2 is  $\sim 1$  at energy  $E \simeq 9$  MeV nucleon<sup>-1</sup> and increases with energy [*Selesnick and Mewaldt*, 1996]. This ratio was measured for  $L$  shells up to 2.1, and it was found to decrease with the geomagnetic latitude down to  $\sim 0.1$ . No other measurements of the isotopic composition of the trapped helium component in radiation belts are available up to now.

[3] Information about hydrogen isotopes is poorer. In the work by *Freden and White* [1960] the observation of four trapped nuclei of tritium in the energy range 126–200 MeV was reported. However, at the same time this experiment, which utilized a small stack of nuclear emulsions, did not observe helium and deuterium nuclei, and that was ascribed by the authors to differences in isotope secondary productions and to a high deuterium interaction cross section. The first observations of real geomagnetically trapped deuterium in the inner radiation belt were presented by *Looper et al.* [1996], performed by Proton-Electron Telescope (PET) on board SAMPEX in the energy range 18–58 MeV nucleon<sup>-1</sup>. In this work it was shown that at the same energy per nucleon the deuterium component is  $\sim 1\%$  of the proton one.

[4] A following work [*Looper et al.*, 1998] reported observations of trapped tritium between 14 and 35 MeV nucleon<sup>-1</sup> at  $L$  shell  $< 1.2$ , with a flux equal to 1/8 of the deuterium one. At higher  $L$  shell values it was not possible to identify tritium nuclei, owing to the increase of the instrument noise.

<sup>1</sup>Moscow Engineering Physics Institute, Moscow, Russia.

<sup>2</sup>Istituto Nazionale di Fisica Nucleare sezione di Roma2, University of Rome "Tor Vergata," Rome, Italy.

<sup>3</sup>Istituto Nazionale di Fisica Nucleare sezione di Trieste, University of Trieste, Trieste, Italy.

<sup>4</sup>Istituto Nazionale di Fisica Nucleare sezione di Bari, University of Bari, Bari, Italy.

<sup>5</sup>Istituto Nazionale di Fisica Nucleare sezione di Firenze, University of Firenze, Firenze, Italy.

<sup>6</sup>Istituto Nazionale di Fisica Nucleare, Laboratori Nazionali di Frascati, Frascati, Italy.

<sup>7</sup>Istituto di Ricerca Onde Elettromagnetiche CNR, Firenze, Italy.

[5] The first hypothesis about the origin of rare light isotopes in radiation belts was that they are generated by the interaction of high-energy trapped protons with the residual atmosphere [Freden and White, 1960]. This source is at least 1 order of magnitude greater than that coming from cosmic ray interactions with air nuclei.

[6] To explain the significant difference between the  ${}^3\text{He}/{}^4\text{He}$  ratios at  $L$  shell  $\approx 1.2$  and at  $L$  shell  $\approx 1.9$  measured by CRRES, it was suggested by Wefel *et al.* [1995] that the interaction region of protons lies at a lower atmospheric altitude for  $L$  shell = 1.2 than for  $L$  shell = 1.9. This implies that for secondary production it is necessary to take into account not only proton interactions with nuclei of helium in the upper atmosphere but also with nuclei of oxygen which dominate at lower altitudes. In the interactions of protons with oxygen the cross section of  ${}^3\text{He}$  production is much larger than that of  ${}^4\text{He}$ .

[7] Detailed calculations by Selesnick and Mewaldt [1996] and comparisons with SAMPEX experimental data show that the atmospheric He source is adequate to account for a substantial fraction of the intensity of the helium isotopes, at  $L$  shell  $\leq 1.2$  and particularly for  ${}^3\text{He}$ . For higher  $L$  shells an additional source of  ${}^4\text{He}$  is required. The model of proton interaction with atmospheric helium is also in agreement with  ${}^3\text{He}$  and  ${}^4\text{He}$  data collected by CRRES at  $L$  shell = 1.2.

[8] While the reactions involving atmospheric helium are reasonably well known, the uncertainties in the cross section value for the reaction with atmospheric oxygen make it difficult to estimate the degree of importance of this additional source. If the interactions with atmospheric oxygen and helium source are combined together, the model gives significantly more  ${}^4\text{He}$  and especially  ${}^3\text{He}$  than that observed by SAMPEX at  $L$  shell = 1.2. For deuterium, instead, the atmospheric He source appears to be somewhat weak to produce the intensities reported by SAMPEX, while the combined calculated intensities for deuterium seem to better reproduce the data.

[9] Selesnick and Mewaldt [1996] suggest that atmospheric oxygen can be a significant source of light isotopes in the inner radiation belt near  $L$  shell = 1.2. At higher  $L$  shells this source may be important only in a narrow range of equatorial pitch angles near the edges of the loss cones, corresponding to the altitude range where oxygen is the dominant component in the atmosphere. Moreover, owing to the different energy spectra of secondary particles produced by proton interactions with O and with He, the oxygen source is relatively more significant than the helium one only for low particle energies up to  $E \sim 10$ –15 MeV nucleon $^{-1}$ .

[10] Another possible mechanism discussed in literature is a radial diffusion of nuclei inside the magnetosphere. In the work by Pugacheva *et al.* [1998] the secondary production rate for  ${}^2\text{H}$ ,  ${}^3\text{H}$ , and  ${}^3\text{He}$  in the upper part of the atmosphere was compared with radial diffusion, and it appeared to dominate at  $L$  shell in the interval  $1.2 \div 1.6$ . The results of the calculations depend on the detailed knowledge of some parameters, such as the radiation belt models and the boundary condition of diffusion equations.

[11] The mission New Instrument for Nuclear Analysis (NINA) presented in this article is the first step of a Russian-Italian scientific program, aimed at studying the

**Table 1.** Energy Windows for Contained Particles in High-Threshold Mode

Particle	Z	Energy, MeV nucleon $^{-1}$
${}^1\text{H}$	1	11–16
${}^2\text{H}$	1	7–13
${}^3\text{H}$	1	5–12
${}^3\text{He}$	2	12–58
${}^4\text{He}$	2	10–50

nuclear component of cosmic rays from H to Fe in the energy range 10–200 MeV nucleon $^{-1}$  in the vicinity of the Earth, by using spaceborne experiments. The instrument NINA was put in orbit aboard the Russian satellite Resurs-01-N4 on 10 July 1998, and during its lifetime it performed measurements of galactic cosmic ray fluxes [Bidoli *et al.*, 2001] and the isotopic composition of solar energetic particles [Bakaldin *et al.*, 2001]. NINA stopped being operational at the middle of the year 1999. On 15 July 2000 a second detector, NINA-2, was placed in orbit housed in the Italian satellite Minisatellite Italiano a Tecnologia Avanzata (MITA), in order to extend NINA measurements in a different phase of the solar cycle.

[12] In this article we report observations of geomagnetically trapped hydrogen and helium isotopes, performed by NINA during passages over the South Atlantic Anomaly (SAA) in the months November 1998 to April 1999, and we give possible interpretations about the origin of radiation belt light isotopes.

## 2. Experimental Device

[13] The telescope NINA is a tower composed of 16 silicon planes, each made of two silicon detectors, segmented in 16 strips orthogonally glued so as to provide the  $X$  and  $Y$  information of the particle track. The first two detectors are 150  $\mu\text{m}$  thick, while the thickness of all the others is 380  $\mu\text{m}$ , for a total of 11.7 mm of silicon.

[14] The main operating trigger of the data acquisition system requires a particle to reach at least the first view ( $X$ ) of the second detector plane. The veto system is performed by setting in anticoincidence the strips 1 and 16 of planes from 2 up to 15 (lateral anticoincidence) and all the strips of plane 16 (bottom anticoincidence). If a particle produces a trigger, signals from detectors are amplified and shaped before analog to digital (ADC) conversion; then the event is stored in a first-in, first-out (FIFO) stack. The data are read by a microprocessor which acquires, processes, and stores the data before the transmission to Earth.

[15] The instrument has two different modes of particle detection: low-threshold and high-threshold mode. In the first configuration the telescope can detect nuclei from hydrogen to iron in the full energy range (10–200 MeV nucleon $^{-1}$ ), whereas in high-threshold mode it is possible to detect hydrogen isotopes only in a narrow energy range (11–16 MeV, see Table 1). About 95% of the mission lifetime measurements were carried out in high-threshold mode, owing to the background conditions (very high proton flux) in the radiation belts.

[16] The segmented structure of the instrument and the measurement of the energy deposit in each silicon strip give the possibility of filtering the background, of reconstructing

**Table 2.** Characteristics of NINA

Characteristic	Value
Geometrical factor	10 cm <sup>2</sup> sr
Maximum aperture	±34°
Pointing accuracy	5°
Time resolution	2 μs
Energy resolution	1 MeV
(containment)	
Mass resolution	H → 0.1 amu He → 0.15 amu

the particle path, and of determining its charge, mass, energy, and incident angle. The optimal performance of NINA is achieved by requesting the full containment of the particle inside the detector, ensured by the lateral and bottom anticoincidence.

[17] The instrument performance was calculated by means of Monte Carlo simulations based on the CERN-GEANT code [Brun *et al.*, 1994]. In addition, the detector was calibrated at several accelerator laboratories, with beam species from hydrogen to oxygen, in a wide energy interval. NINA geometrical factor for helium and hydrogen isotopes is ~10 cm<sup>2</sup>sr, decreasing as a function of energy in the energy interval 10–50 MeV nucleon<sup>-1</sup>. The mass resolution of the instrument is ~0.15 amu for He isotopes and ~0.1 amu for H isotopes. The energy resolution is ~1 MeV. A detailed description of the instrument and its performance in orbit are reported in the works by Bakaldin *et al.* [1997] and Bidoli *et al.* [1999, 2001]. Some characteristics of the detector are summarized in Table 2.

### 3. Data Analysis and Observations

[18] The satellite Resurs-01-N4 has a near-Earth polar orbit with inclination 98° and altitude 835 km. It makes ~14 revolutions per day, and when the orbit crosses the South Atlantic Anomaly (~7 times per day), NINA can measure particles trapped in the inner radiation belt. The period of observation taken under consideration ranges from November 1998 to April 1999; data include also particles collected during solar energetic particle events, because even in conditions of intense solar activity, the fluxes measured by NINA in the inner radiation belt remain practically constant.

[19] The study of rare isotope abundances in SAA requires a careful analysis of the data collected. The background includes both noise and events not identifiable and particles produced by secondary interactions in the material around NINA. The segmented structure of the detector allows a very precise determination of the particle path inside the instrument to be reached. By a dedicated off-line track selection algorithm [Bidoli *et al.*, 2001], upward moving particles, nuclear interaction events, and multiple tracks are discarded; by this selection not more than 3% of good tracks are rejected. The efficiency reduction capability of the track selection algorithm was previously tested on accelerator data and in the galactic cosmic rays analysis [Bidoli *et al.*, 2001].

[20] Figure 1 shows a  $E_1$  versus  $E_{\text{tot}}$  diagram ( $E_1$  is the energy released by the particles in the first silicon detector of the tower NINA, and  $E_{\text{tot}}$  is the total energy released in

the whole instrument) for events collected in SAA, after the action of the track selection. Lines corresponding to different isotopes are visible. Charge and mass identification procedures are applied to events which survive the track selection algorithm.

[21] The mass  $M$  and the charge  $Z$  of the particles are calculated in parallel by two methods: (1) the method of the residual range [Cook *et al.*, 1993; Hasebe *et al.*, 1993] and (2) the method of the approximation to the Bethe-Bloch theoretical curve.

[22] In method 1 the charge  $Z$  is estimated by means of the product  $E_1 \times E_{\text{tot}}$ , and the mass is evaluated by applying the following formula:

$$M = \left( \frac{a \left[ E_{\text{tot}}^b - (E_{\text{tot}} - \Delta E)^b \right]}{Z^2 \Delta x} \right)^{\frac{1}{b-1}}, \quad (1)$$

where  $\Delta E$  is the energy lost by the particle in a thickness  $\Delta x$  measured starting from the first plane. A precise evaluation of parameters  $a$  and  $b$  for each atomic species has been obtained both from real and simulated data [Bidoli *et al.*, 1999].

[23] With method 2 we estimate the mass  $M$  and charge  $Z$  of the particle by minimizing the following  $\chi^2$  quantity:

$$\chi^2 = \sum_{i=1}^N [W_i (\Delta E_i^{\text{real}} - \Delta E_i^{\text{theor}})]^2, \quad (2)$$

where  $\Delta E_i^{\text{real}}$  is the energy released by the particle in the  $i$ th view,  $\Delta E_i^{\text{theor}}$  is the corresponding expected value,  $W_i$  is the weight for every difference  $W_i = \frac{1}{\Delta E_i^{\text{real}}}$ , and the sum is extended to the  $N$  silicon layers activated by the particle, excluding the last one where the particle stops and the fluctuations of the energy deposits are generally very big.

[24] For a complete rejection of the background, only particles with the same final identification given by the two

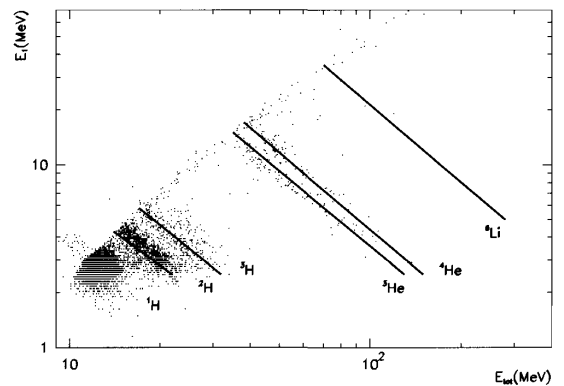


**Figure 1.**  $E_1$  versus  $E_{\text{tot}}$  diagram for events collected in the South Atlantic Anomaly (SAA).  $E_1$  is the energy released by the particles in the first silicon detector of the tower NINA, and  $E_{\text{tot}}$  is the total energy released in the whole instrument.

methods are selected. Finally, a cross check between the real range of the particle in the detector and the expected value according to simulation is a consistency test for the event.

[25] NINA is accommodated on Resurs in order to point always toward the zenith. The angle accuracy of the satellite axis is  $\sim 1^\circ$ . By the knowledge of the spacecraft orientation and the incoming particle direction in the telescope, NINA is able to determine the particle pitch angle with an accuracy of  $\sim 5^\circ$ . Figure 2 presents the local pitch angle ( $\alpha_{loc}$ ) distribution for particles detected by NINA in the region  $L$  shell  $< 1.2$  and magnetic field  $B < 0.22$  G (SAA region). This distribution is peaked at  $90^\circ$ . The average value of  $\alpha_{loc}$  observed by NINA in this region corresponds to an average equatorial angle  $\alpha_0$  of  $\sim 75^\circ$ . Calculations of particle trajectories with  $\alpha_{loc}$  of  $\sim 90^\circ$ , at Resurs altitudes and knowing the  $L$  shell value, show that these particles can be geomagnetically trapped because mirror points are higher than atmospheric altitudes ( $\sim 200$  km). The estimated lifetime for trapped  $^4\text{He}$  at  $L$  shell = 1.2 is more than 1 year [Selesnick and Mewaldt, 1996].

[26] Figure 3 (left) presents the mass distribution for  $^3\text{He}$  and  $^4\text{He}$  in the SAA region, for data collected in the time period considered. It is possible to see the good separation between isotopes and the higher abundance of  $^3\text{He}$  with respect to  $^4\text{He}$ , in agreement with previous observations [Wefel et al., 1995]. Figure 3 (right) shows the mass distribution for hydrogen isotopes.

[27] The most delicate point in analyzing rare isotope abundances is to understand whether these nuclei are particles really trapped by the geomagnetic field or are due to secondary production inside the instrument. The detector is installed into a special vessel having a  $300 \mu\text{m}$  aluminum window in correspondence with the telescope aperture. Our data of solar energetic particle (SEP) events confirm that the interactions of low-energy protons and heliums with the aluminum window cannot produce a number of secondary  $^3\text{He}$  nuclei such as that observed in the SAA; our average  $^3\text{He}/^4\text{He}$  ratio measured during SEP events was  $\sim 0.01$  [Bakaldin et al., 2001]. However, the energy of protons trapped in the inner radiation belt extends up to 1 GeV, much beyond typical SEP energies; since the interaction cross section increases with energy, the contribution of the high-energy part of the proton spectrum could be important. For cosmic ray observations over the polar caps we have seen a clear evidence of local secondary production: in the mass distribution of hydrogen isotopes, indeed, there was a tritium peak, evidently not of galactic origin because of its small half-life ( $\sim 12.5$  years).

[28] The cross-section value of proton interaction in the Al window, however, remains uncertain, so that it is not possible to calculate the number of secondaries in the instrument with high accuracy. It is also difficult to distinguish the secondary production inside the instrument, because usually the reaction produces more than one particle with a complex energetic and spatial distribution. Therefore, to estimate the secondary isotope fraction, we utilized a method similar to that proposed by Looper et al. [1996] for PET telescope. In this technique we consider the first detector of NINA as a silicon target  $150 \mu\text{m}$  thick; comparing the particles surviving the track selection algorithm in the two cases, including and not including the first silicon layer, we have in the second case an additional

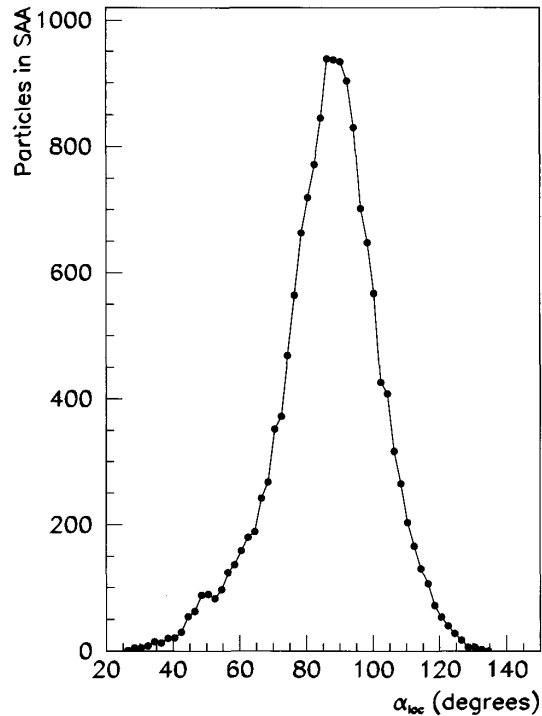


**Figure 2.** Distribution of the local pitch angle  $\alpha_{loc}$  for particles detected in the region  $L$  shell  $< 1.2$  and  $B < 0.22$  G (SAA).

number of secondary particles, which were presumably originated in the silicon target. If we reasonably suppose that the cross section of light isotopes generation in Si and Al are similar, then it is possible to estimate the number of secondaries generated in the aluminum window starting from the number of secondaries produced in the silicon, just by considerations of thickness and density of the two materials. The geometrical factor in the two cases is practically the same, owing to the small thickness of the first layer; the ratio  $R$  between the particles produced in the silicon target ( $150 \mu\text{m}$  thick) and in the aluminum window ( $300 \mu\text{m}$ ) is finally  $R = 0.43$ . This method was tested for cosmic rays detected in polar caps; after the subtraction of the estimated background the tritium peak practically disappeared.

[29] In Figure 3 the shaded areas represent the background contribution calculated in this way, for helium (left) and hydrogen (right). The comparison between this contribution and the measured abundances shows that NINA detected hydrogen and helium isotopes geomagnetically trapped.

#### 4. Results and Interpretations

[30] The energy spectra of  $^3\text{He}$  and  $^4\text{He}$  obtained by NINA at  $L$  shell  $1.18 \div 1.22$  and  $B < 0.22$  G are presented in Figure 4, together with the data of MAST from SAMPEX at  $L$  shell = 1.2. Fluxes are averaged over local pitch angles at

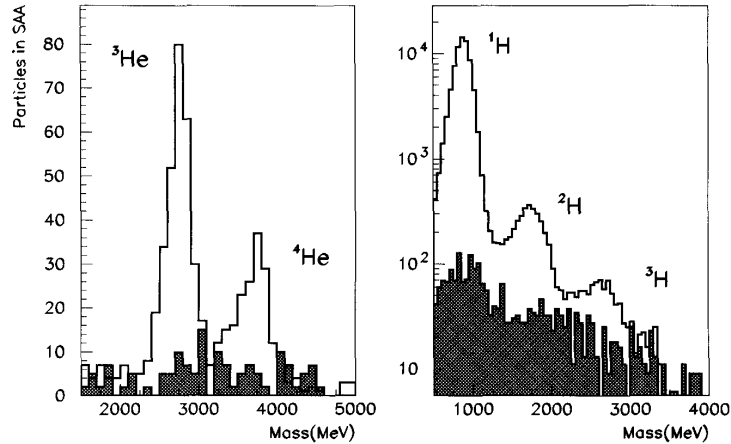


**Figure 3.** Mass distributions for geomagnetically trapped (left) He and (right) H isotopes measured at  $L$  shell  $< 1.2$  and  $B < 0.22$  G. The shaded area represents the estimated background.

$\sim 800$  km and  $\sim 600$  km of altitude for NINA and MAST, respectively. The  $^3\text{He}$  spectrum is fitted by a power law with index equal to  $2.30 \pm 0.08$  in the energy range 12–50 MeV nucleon $^{-1}$ , while  $^4\text{He}$  has a spectral index of  $3.4 \pm 0.2$  in 10–40 MeV nucleon $^{-1}$ . The NINA and MAST data have been gathered during quite different periods of the solar cycle; taking also into account the sharp decrease of the trapped particles flux near the edge of the radiation belts, they show a reasonable agreement.

[31] The energy spectra of  $^3\text{He}$  and  $^4\text{He}$  presented in Figure 4 are in good agreement with calculations for

atmospheric helium source (dotted and solid lines, for two different equatorial pitch angles). The thick line is the sum of the  $p + \text{He}$  and  $p + \text{O}$  contributions, which seems to overestimate the  $^3\text{He}$  contents with respect to the experimental measurements.

[32] From fluxes of Figure 4 we derived the  $^3\text{He}/^4\text{He}$  ratio as a function of energy, shown in Figure 5; the dotted line is the theoretical calculation for atmospheric oxygen source at  $\alpha_0 = 80^\circ$ , while the solid and dashed lines correspond to the helium source secondary production at two different equatorial pitch angles,  $\alpha_0 = 60^\circ$  and  $\alpha_0 = 80^\circ$ . From this picture

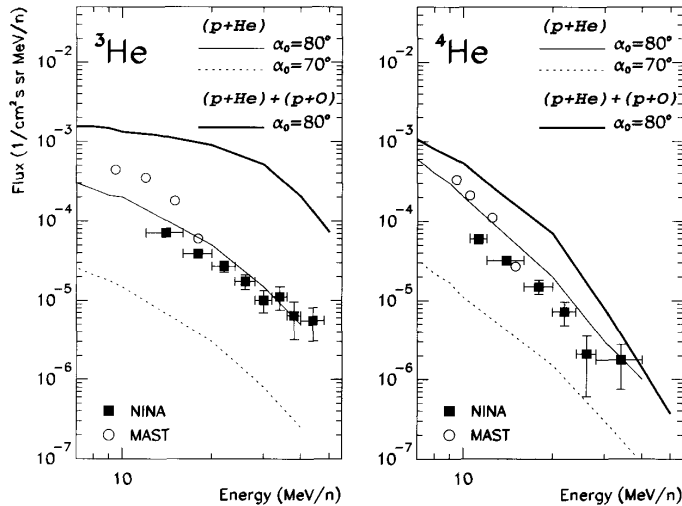


**Figure 4.** The (left)  $^3\text{He}$  and (right)  $^4\text{He}$  differential energy spectra measured inside the SAA by NINA (squares) and MAST (circles). The solid and dotted lines represent the calculated helium flux at equatorial pitch angles  $\alpha_0 = 80^\circ$  and  $\alpha_0 = 70^\circ$ , respectively, assuming atmospheric helium as the source of secondary production [Selesnick and Mewaldt, 1996]. The thick line is the sum of the  $p + \text{He}$  and  $p + \text{O}$  contributions at  $\alpha_0 = 80^\circ$ .

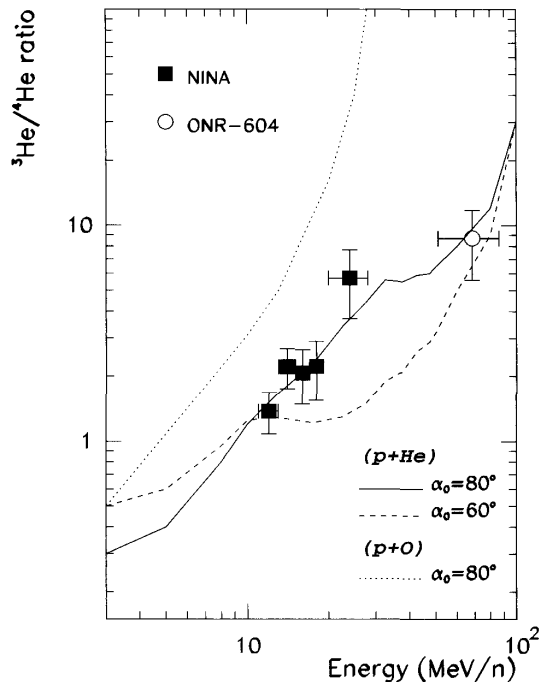


**Figure 5.** The  ${}^3\text{He}/{}^4\text{He}$  ratio at  $L$  shell = 1.2 measured by NINA (squares) and by ONR-604 (circle) [Wefel *et al.*, 1995]. The dotted line represents the calculated ratio for the reaction  $p + O$ . The solid and dashed lines represent the calculated ratio for the reaction  $p + \text{He}$  at pitch angles  $\alpha_0 = 80^\circ$  and  $\alpha_0 = 60^\circ$ , respectively [Selesnick and Mewaldt, 1996].

it is possible to conclude that the model of proton interaction with oxygen in atmosphere overestimates the  ${}^3\text{He}$  production. That is not surprising because, as mentioned by the authors themselves [Selesnick and Mewaldt, 1996], the lack of cross-section data and the forward scattering approximation can probably lead for an O source to an overestimate of the trapped particle source rate.

[33] NINA measured  ${}^3\text{He}/{}^4\text{He}$  ratio, averaged in the energy interval 10–30 MeV nucleon $^{-1}$ , is equal to  $2.2 \pm 0.2$  for local pitch angles  $\alpha_{\text{loc}}$  in the range  $80^\circ \div 90^\circ$ , and  $2.1 \pm 0.4$  for  $\alpha_{\text{loc}}$   $50^\circ \div 70^\circ$ , so it does not show an appreciable variation as a function of the pitch angle. Calculations indicate instead that the isotope intensity from an atmospheric source should peak at a pitch angle corresponding to the altitude where this source is the dominant atmospheric constituent [Selesnick and Mewaldt, 1996]. In the range  $\alpha_{\text{loc}}$   $50^\circ \div 70^\circ$  the mirror points of the particles lie at altitudes where oxygen dominates in atmosphere, so this is a further indication that oxygen seems not to be the dominant source of secondary production in this energy range.

[34] Fluxes of  ${}^2\text{H}$  and  ${}^3\text{H}$  obtained by NINA at  $L$  shell 1.18  $\div$  1.22 and  $B < 0.22$  G are presented in Figure 6, for the energy range shown in Table 1. Fluxes are compared to calculations for atmospheric helium source (dotted and solid

lines, for two different equatorial pitch angles) and for the sum of the  $p + \text{He}$  and  $p + O$  contributions (dashed line), and to the model that combines secondary production in atmosphere and radial diffusion (thick line).

[35] The deuterium flux shows a reasonable agreement with calculations; a deeper analysis, nevertheless, reveals that the sum of the  $p + \text{He}$  and  $p + O$  reaction does not provide a sufficient deuterium intensity, as already pointed out by Selesnick and Mewaldt [1996] and Pugacheva *et al.* [1998], who compared calculations with SAMPEX data. Figure 6 presents, in fact, fluxes averaged over a  $L$  shell interval, but fluxes around the boundary of radiation belts have a very steep dependence on the  $L$  shell value. More reliable measurements are therefore ratios between different species. Our measured  ${}^2\text{H}/{}^1\text{H}$  ratio is roughly equal to 1% at energy  $\sim 10$  MeV nucleon $^{-1}$ , and it is close to that observed by PET instrument at 18–58 MeV nucleon $^{-1}$  [Looper *et al.*, 1996]. The calculation of Selesnick and Mewaldt [1996] predicts instead a ratio of  $\sim 10^{-3}$  at these energies, for  $L$  shell = 1.2.

[36] NINA measured  ${}^2\text{H}/{}^3\text{H}$  ratio at 10 MeV/n is  $\sim 4$ , roughly 2 times lower than that measured by SAMPEX at higher energies, but this may be explained by the differing production cross sections of  ${}^2\text{H}$  and  ${}^3\text{H}$  as a function of energy, inferred for instance by data in the work of Wu *et al.* [1979]. From Figure 6 it is visible that the  ${}^2\text{H}/{}^3\text{H}$  ratio calculated by Pugacheva *et al.* [1998] increases with energy, but its minimum value is  $\sim 30$ .

[37] In order to estimate the  ${}^3\text{He}/{}^3\text{H}$  ratio, since the two isotope measurements span two different energy regions in NINA detector (see Table 1), it is necessary to extrapolate the  ${}^3\text{He}$  flux, presented in Figure 4, in the tritium energy region. The  ${}^3\text{He}/{}^3\text{H}$  ratio has a value of  $\sim 2$ .

[38] Figure 7 shows the behavior of the deuterium flux reconstructed by NINA as a function of  $L$  shell. Data were normalized because experimental points refer to pitch angles  $\alpha_0 \sim 75^\circ$ , while the calculations were performed for  $\alpha_0 = 90^\circ$ . The picture presents also flux calculations for the reactions  $p + O$  and  $p + \text{He}$ , as well as with the flux obtained combining secondary production in atmosphere and radial diffusion in inner radiation belts. The curves show that the contribution from the reaction  $p + O$  peaks at  $L$  shell  $\simeq 1.15$ , whereas the  $p + \text{He}$  production is equally distributed in the whole range of  $L$  shell  $< 1.3$ . Since NINA data do not show any evident peak in flux in the proximity of  $L$  shell  $\simeq 1.15$ , this is again a confirmation that the reaction  $p + O$  plays a minor role in the formation of trapped light isotopes with energy greater than 10 MeV nucleon $^{-1}$  in the inner radiation belt.

## 5. Conclusion

[39] Results presented in this work show that rare light isotopes represent a distinct component of the Earth's inner radiation belt. Geomagnetically trapped fluxes of  ${}^2\text{H}$ ,  ${}^3\text{H}$ ,  ${}^3\text{He}$ , and  ${}^4\text{He}$  were measured by the instrument NINA aboard the satellite Resurs, for  $L$  shell  $\sim 1.2$  at  $\sim 800$  km of altitude. The  ${}^2\text{H}/{}^1\text{H}$  ratio at energy 10 MeV nucleon $^{-1}$  was  $\sim 0.01$ , the  ${}^3\text{H}/{}^2\text{H} \sim 0.2$ , and the  ${}^3\text{He}/{}^3\text{H}$  ratio  $\sim 2$ . The  ${}^3\text{He}/{}^4\text{He}$  ratio increases from  $\sim 1$  to  $\sim 5$  across the energy range 10–40 MeV nucleon $^{-1}$ . The data analysis and the comparison with the available theoretical calculations bring one to the con-

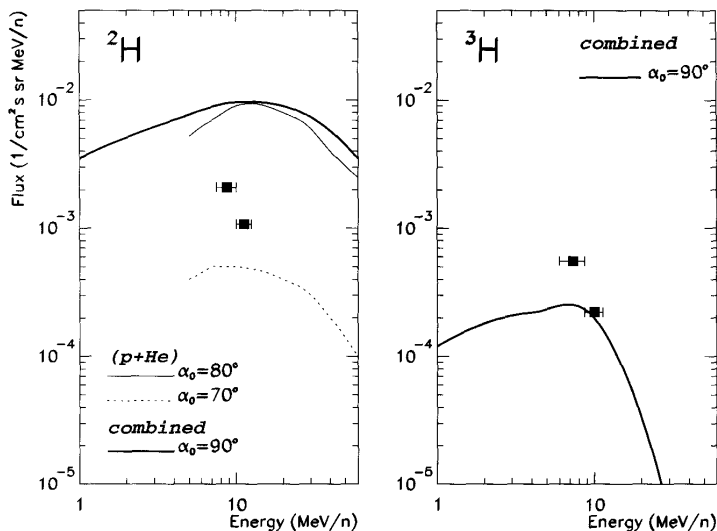


**Figure 6.** The (left)  $^2\text{H}$  and (right)  $^3\text{H}$  differential energy spectra measured inside the SAA by NINA. The solid and dotted lines represent the calculated helium flux at equatorial pitch angles  $\alpha_0 = 80^\circ$  and  $\alpha_0 = 70^\circ$ , respectively, assuming atmospheric helium as the source of secondary production [Selesnick and Mewaldt, 1996]. The dashed line is the sum of the  $p + \text{He}$  and  $p + \text{O}$  contributions at  $\alpha_0 = 80^\circ$ , while the thick line comes from calculations by [Pugacheva et al., 1998], at  $\alpha_0 = 90^\circ$ .

clusion that the light isotopes component originated from the interactions of high-energy trapped protons with the residual atmosphere. At energy above  $10 \text{ MeV nucleon}^{-1}$  at the altitude of Resurs, the interaction with atmospheric helium seems to dominate with respect to oxygen.

[40] The observed  $^2\text{H}/^1\text{H}$  and  $^3\text{H}/^2\text{H}$  ratios at energy  $10 \text{ MeV nucleon}^{-1}$  are higher than calculated from atmospheric production models. The results of the calculations, however, depend on the detailed knowledge of some physical parameters, such as the radiation belt models, the atmos-

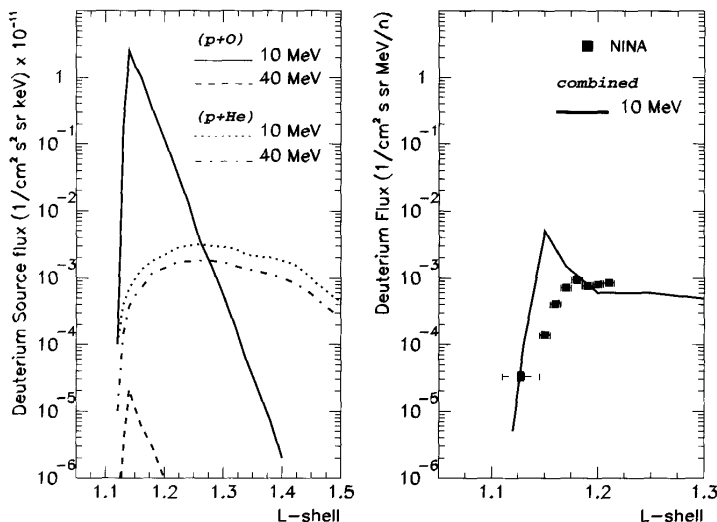


**Figure 7.** (left) Calculations for secondary production of deuterium at different energies for different reactions [Selesnick and Mewaldt, 1996]. (right) Experimental deuterium flux as a function of  $L$  shell measured by NINA in the energy range  $7\text{--}13 \text{ MeV nucleon}^{-1}$ , together with calculations from the combined action of secondary production and radiation belt radial diffusion at  $10 \text{ MeV}$  made by [Pugacheva et al., 1998].

pheric density model, and cross-section parameterization, and also on the solar cycle phase. The measurements performed by NINA, and those that will be added by NINA-2, can provide new inputs to the theoretical calculations.

[41] **Acknowledgments.** We acknowledge the Russian Foundation of Base Research, grant 99-02-16274, who partially supported the Russian Institutions for this work.

## References

- Bakaldin, A., et al., Experiment NINA: Investigation of low energy nuclear fluxes in the near-Earth space, *Astroparticle Phys.*, 8, 109, 1997.
- Bakaldin, A., et al., Light isotope abundances in solar energetic particles measured by the space instrument NINA, *astro-ph/0106390*, Int. Sch. for Adv. Stud., Trieste, Italy, 2001.
- Bidoli, V., et al., The space telescope NINA: Results of a beam test calibration, *Nucl. Instrum. Methods Phys. Res., Sect. A*, 424, 414, 1999.
- Bidoli, V., et al., In-orbit performances of the space telescope NINA and GCR flux measurements, *Astrophys. J., Suppl. Ser.*, 132, 365, 2001.
- Brun, R., et al., GEANT detector description and simulation tool, *W5014*, Comput. and Networks Div., Eur. Org. for Nucl. Res., Geneva, Switzerland, 1994.
- Cook, W. R., et al., MAST: A mass spectrometer telescope for studies of the isotopic composition of solar, anomalous and galactic cosmic ray nuclei, *IEEE Trans. Geosci. Remote Sens.*, 31-3, 531, 1993.
- Freden, S. C., and R. S. White, Particle fluxes in the inner radiation belt, *J. Geophys. Res.*, 65, 1377, 1960.
- Hasebe, N., et al., Improvement of mass resolution of cosmic ray nuclei using a  $\Delta E \times E$  Si detector telescope, *Nucl. Instrum. Methods Phys. Res., Sect. A*, 325, 335, 1993.
- Krimigis, S. M., and J. A. Van Allen, Geomagnetically trapped alpha particles, *J. Geophys. Res.*, 72, 5779, 1967.
- Looper, M. D., J. B. Blake, J. R. Cummings, and R. A. Mewaldt, SAMPEX observations of energetic hydrogen isotopes in the inner zone, *Radiat. Meas.*, 26, 967, 1996.
- Looper, M. D., J. B. Blake, and R. A. Mewaldt, Maps of hydrogen isotopes at low altitudes in the inner zone from SAMPEX observations, *Adv. Space Res.*, 21, 1679, 1998.
- Pugacheva, G. I., et al., Hydrogen and helium isotope inner radiation belts in the Earth's magnetosphere, *Ann. Geophys.*, 16, 931, 1998.
- Selesnick, R. S., and R. A. Mewaldt, Atmospheric production of radiation belt light isotopes, *J. Geophys. Res.*, 101, 19,745, 1996.
- Wefel, J. P., et al., The isotopic composition of geomagnetically trapped helium, *Proc. Int. Conf. Cosmic Rays 24th*, 4, 1021, 1995.
- Wu, J. R., C. C. Chang, and H. D. Holmgren, Charged-particle spectra: 90 MeV protons on  $^{27}\text{Al}$ ,  $^{58}\text{Ni}$ ,  $^{90}\text{Zr}$  and  $^{209}\text{Bi}$ , *Phys. Rev. C*, 19, 698, 1979.
- O. Adriani, P. Papini, P. Spillantini, S. Straulino, and E. Vannuccini, INFN sezione di Firenze, University of Firenze, Largo Enrico Fermi 2, I-50125 Firenze, Italy.
- M. Ambriola, R. Bellotti, F. Cafagna, M. Circella, and C. De Marzo, INFN sezione di Bari, University of Bari, Via Amendola 173, I-70126 Bari, Italy.
- A. Bakaldin, A. Galper, S. Koldashov, M. Korotkov, A. Leonov, V. Mikhailov, A. Murashov, and S. Voronov, Moscow Engineering Physics Institute, Kashirskoe Shosse 31, 115409 Moscow, Russia.
- V. Bidoli, M. Casolino, M. De Pascale, G. Furano, A. Iannucci, A. Morselli, P. Picozza, and R. Sparvoli, INFN sezione di Roma2, University of Rome "Tor Vergata," Via della Ricerca Scientifica 1, I-00133 Rome, Italy. (Roberta.Sparvoli@roma2.infn.it)
- M. Boezio, V. Bonvicini, R. Cirami, A. Vacchi, and N. Zampa, INFN sezione di Trieste, University of Trieste, Via A. Valerio 2, I-34147 Trieste, Italy.
- G. Castellini, Istituto di Ricerca Onde Elettromagnetiche CNR, Via Panciatichì 64, I-50127 Firenze, Italy.
- M. Ricci, INFN Laboratori Nazionali di Frascati, Via Enrico Fermi 40, I-00044 Frascati, Italy.